Spin resonance in the ordered magnetic state of $Ni_5(TeO_3)_4Cl_2$

L. Mihály,[1,2] T. Fehér,[3,4] B. Dóra,[2] B. Náfrádi,[3] H. Berger,[3] and L. Forró[3]
[1]*Department of Physics and Astronomy, Stony Brook University, Stony Brook, New York 11794-3800, USA*
[2]*Electron Transport Research Group of the HAS and Department of Physics, Budapest University of Technology and Economics, P.O. Box 91, H-1521 Budapest, Hungary*
[3]*Ecole Politechnique Federale, Lausanne CH-1015, Switzerland*
[4]*Solids in Magnetic Fields Research Group of the HAS and Institute of Physics, Budapest University of Technology and Economics, P.O. Box 91, H-1521 Budapest, Hungary*
(Received 28 June 2006; revised manuscript received 22 August 2006; published 2 November 2006)

The transition metal tellurium oxychloride, $Ni_5(TeO_3)_4Cl_2$, has been investigated by high-field electron-spin resonance for frequencies up to 3 THz, at temperatures well below the magnetic ordering at 23 K. At zero external field several resonance modes have been identified. When the applied magnetic field is perpendicular to both the **a** and **b** crystallographic directions, one of the magnetic-resonance modes softens, and a spin-flop transition occurs around 10 T. The results are discussed in terms of the crystal structure, and compared to other magnetically ordered materials with multiple magnetic sublattices, including orthoferrites and triangular antiferromagnets.

DOI: 10.1103/PhysRevB.74.174403 PACS number(s): 76.50.+g, 75.50.Ee

I. INTRODUCTION

Quantum fluctuations may play an important role in the ground-state properties of a spin system of reduced dimensionality or frustrated interactions, especially if the constituent spins have a low (close to spin 1/2) value.[1] On the other hand, the spin-orbit coupling, resulting in the single-ion anisotropy, the exchange anisotropy, the Dzyaloshinski-Moriya interaction, or similar terms in the effective Hamiltonian, usually introduces a gap into the magnon spectrum. Finite magnon energies lead to less quantum fluctuations and a more stable classical spin order. The properties of the gap can be explored by studying the field dependence of the electron-spin resonance. In single crystals, the field dependence of the resonance frequency for magnetic field applied in different crystallographic directions can be used to determine the nature of the spin-lattice coupling.[2,3]

In search for magnetic systems with reduced dimensionality two transition-metal tellurium oxychlorides have been synthesized recently,[4] with the general formula $Ni_5(TeO_3)_4X_2$ (X=Cl,Br). $Ni_5(TeO_3)_4Cl_2$, the subject of our study, exhibits a magnetic phase transition at 23 K, and a negative Curie-Weiss temperature ($\Theta=-50$ K) in the paramagnetic state, indicating antiferromagnetic interactions. The nickel ions in $Ni_5(TeO_3)_4Cl_2$ have a $3d^8$ electronic configuration, with spin 1, forming a quasi-two-dimensional magnetic structure.[4] The crystal is monoclinic, of space group $C2/c$ with unit-cell dimensions $a=19.5674$ Å, $b=5.2457$ Å, $c=16.3084$ Å, and $\beta=125.3°$ (Fig. 1).

II. EXPERIMENT

The single crystals used in this study were grown by the usual halogen vapor transport technique, using HCl or HBr as transport agents. The charge and growth-zone temperatures were 750 and 550 °C, respectively. Orange colored, semitransparent crystals of maximum size $10\times10\times0.2$ mm were obtained. The stoichiometry was quantitatively probed by electron-probe microanalysis, and the structure was characterized by x-ray diffraction. The electron spin resonance (ESR) measurements were performed on an oriented single-crystal sample of dimensions $10\times3\times0.2$ mm. According to the Laue diffractogram, the **a** and **b** directions

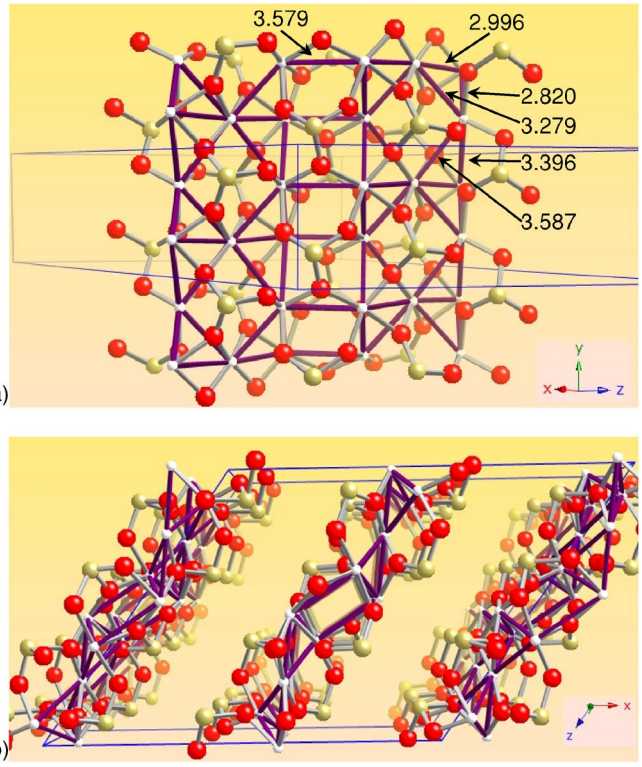

FIG. 1. (Color online) Structure of $Ni_5(TeO_3)_4Cl_2$. The numbers indicate Ni-Ni distances in Å. Gray, red, and yellow colors correspond to Ni, O, and Te atoms, respectively. The unit cell is outlined in blue. Purple bonds emphasize the Ni lattice. (a) The two-dimensional $Ni_5Te_4O_{12}$ sheets. (b) Side view of the $Ni_5Te_4O_{12}$ sheets. The chlorine (not shown) occupies the space between the sheets.

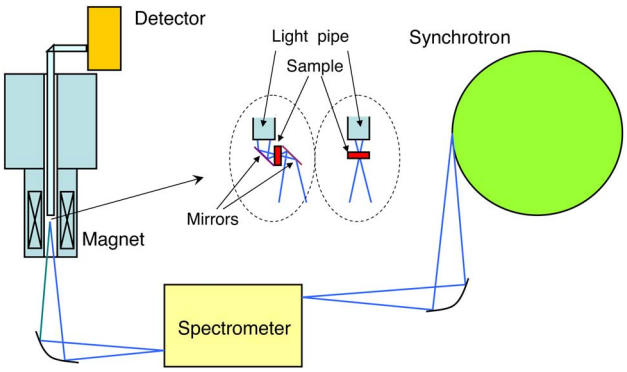

FIG. 2. (Color online) Schematic representation of the measurement setup. The two sample holders are sketched in the center. The **a**-**b** plane of the sample is either parallel (left inset) or perpendicular to (right inset) the external field. In the first case the static field is in the **a**-**b** plane, and its direction relative to the sample was chosen to be either parallel to **a** or parallel to **b**. The incident light is always perpendicular to the plane of the sample. The polarization of the light at the sample is set to parallel to **a** or **b** by rotating the whole sample holder around its vertical axis.

are parallel to the edges of the slab, with **b** along the 10-mm side. To facilitate further discussions, we define $\mathbf{c}^*$ as the direction perpendicular to both **a** and **b**.

The spin-resonance measurements were performed in transmission geometry at Stony Brook University's high magnetic field/infrared facility at the U12 IR beamline of the National Synchrotron Light Source.[3] The broad band ("white") far-IR radiation from the synchrotron was focused to the "external source" port of the spectrometer. There was a polarizer at the exit port of the spectrometer, and another set of mirrors guided the light to the sample, along the vertical axis of the magnet (see Fig. 2). The light transmitted by the sample was collected into a light pipe, and guided to the detector, on the top of the magnet.

The light always passed through the sample in the $\mathbf{c}^*$ direction, perpendicular to the **a**-**b** plane. Two sample holders were constructed for orienting the sample relative to the external static magnetic field **H**. For $\mathbf{H}\|\mathbf{c}^*$ the sample holder was simple: the sample was set flat on a horizontal disc with a hole in the center (see Fig. 2, right inset). The direction of the polarization of the incident light was controlled by rotating the whole sample holder around its vertical axis. For **H** in the **a**-**b** plane the sample holder had a mirror turning the light beam horizontal at the sample, and a second mirror reflecting it back into the vertical light pipe (see Fig. 2, left inset). The sample was mounted on a vertical disc, so that either the **a** or the **b** direction was vertical. Again, the polarization of the light at the sample was set to horizontal or vertical by rotating the whole sample holder around its vertical axis.[5] The measurement configurations were tested by placing an analyzer in the sample position. The polarization state of the light was well maintained by the optics. When referring to the direction of the polarization, we always mean the direction of the oscillating *magnetic* field vector (as opposed to the electric field, commonly considered in optical spectroscopy).

Each measurement was performed with two beamsplitters. A 125-μm-thick mylar beamsplitter was employed to

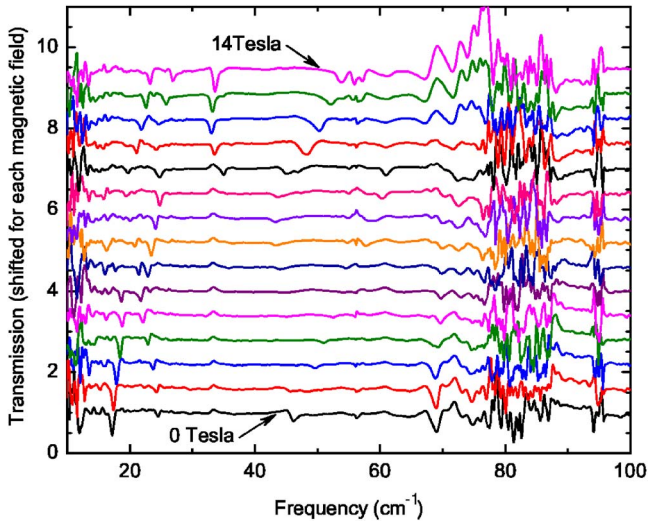

FIG. 3. (Color online) Representative spectra at 2.5 K, taken with the Ge coated mylar beamsplitter. The static field was perpendicular to the **a**-**b** plane of the sample and the polarization was parallel to **a**. The noise around 80 cm^{-1} is due to strong phonon absorption, causing diminishing intensity in that spectral range.

reach to the lowest frequencies, 8 cm^{-1}, available with the spectrometer. This beamsplitter has vanishing efficiency around integer multiples of 25 cm^{-1}, but it provides excellent sensitivity otherwise. A Ge-coated mylar beamsplitter was used to cover a wide range of frequencies, ranging from 15 to 120 cm^{-1}. The absolute upper frequency limit (120 cm^{-1}) was due to the cold filter in the He-cooled bolometer detector, but the phonon and multiphonon absorption in the sample became also very strong above 100 cm^{-1}. The data were recorded at 2.5 or 3.0 K, well below 23 K, the temperature of the magnetic ordering transition.

At each setting the field dependence of the transmitted light was measured. In a typical measurement the sample was cooled in zero field, and spectra were taken in 0.5-T steps, starting at $H=0$ T and finishing at $H=14$ T. The polarization of the light was rotated by 90°, and the measurement was repeated. Then the beamsplitter was changed in the spectrometer and the whole procedure was repeated.

The raw transmission intensity is determined by the incident spectrum, the spectrometer transfer function, the windows on the magnet, the transmission of the sample, and the sensitivity of the detector. The transmission of the sample, in turn, has features independent of the magnetic field (phonons, scattering, and absorption due to impurities) and field-dependent features (spin resonance, possibly other phonons that are coupled to spins).

We eliminated the field-independent properties by taking the average of all 29 spectra belonging to different magnetic fields at any given setting and dividing each spectrum with the average. Figure 3 shows a set of representative "transmission" data obtained this way. Spin resonant absorption shows up as dips in the transmission curves at certain frequencies. The enhanced noise at the low end of the spectral range is due to the drop of the sensitivity of the instrument. The result is also dominated by the noise in any frequency regime when the intensity is low due to strong phonon absorption in the

sample. The peaks and valleys and noise at 58, 70–88, and 95 cm^{-1} are due to the presence of phonons that are, in a good approximation, independent of the magnetic field. At 58 and 95 cm^{-1} the phonons are narrow, and the intensity of the detected light approaches zero in a narrow range of frequencies only. In the 70–88-cm^{-1} spectral range there are several strong phonons, totally blocking the light for a rather wide frequency range. The phonon features exhibit strong dependence on the polarization of the incident light. We did not see evidence for magnetic-field-dependent phonon line positions, as expected in multiferroic materials.[6] Since we are primarily interested in spin resonance, we did not investigate the phonons in detail.

The transmission curves were converted into two-dimensional field-frequency maps, where the darker shades correspond to a more intense magnetic absorption. The advantage of these maps, compared to the spectra shown in Fig. 3, is that the weaker features are more visible to the human eye if seen in the context of their environments. Figures 4–6 show the field-frequency maps for external field parallel to **a**, **b**, and $\mathbf{c}^*$, respectively. Two polarization directions are shown for each field direction. Data taken with the two beamsplitters look essentially similar, except for the sensitivity differences in different frequency ranges.

In zero field the spin resonance depends only on the polarization of the light, and it is expected to be identical for the three sets of data presented in Figs. 4–6. In practice, there may be minor differences in the data sets, due to the evaluation of the data. For example, if a spin-resonance mode happens to be entirely independent of the external field for a certain field direction (not happening here, but theoretically possible), then our evaluation process would miss that mode. However, the same mode would show up in the other two data sets with fields applied in different directions, when the mode frequency depends on the field. Also, some modes may have vanishing (or very small) transition matrix elements in zero field. The zero-field frequency of such modes can be determined only by extrapolation from finite field to zero. Some of the zero-field resonance frequencies correspond to degenerate modes, splitting into two resonances in finite field. A summary of the zero-field modes is shown in Table I.

The measurement with field and polarization along the **a** direction (Fig. 4) had a slightly diminished sensitivity due the imperfect alinement of the light beam relative to the sample. In one data set obtained with the Ge-coated mylar beamsplitter the data for fields larger than 12 T were corrupted. Nevertheless, at least two field-dependent magnetic resonance lines (modes 6 and 7, starting at $\omega_6=32.2$ cm^{-1} and $\omega_7=46$ cm^{-1}) are visible in the **a**/**a** configuration. For the other polarization (labeled **a**/**b** in the figure) the mode-6 mode is not visible at zero field, but it becomes active in finite fields. Mode 7 is very strong. The crossover of these two modes around 11 T is evident in both polarizations. The frequency of mode 2 is nearly independent of the field, the frequency of mode 3 increases with field. Mode 10 splits into two resonances at finite field, and there is also a faint mode that extrapolates to $\omega_9=63$ cm^{-1} in zero field.

For field and polarization along the **b** direction (Fig. 5) modes 10 and 8 (starting at $\omega_{10}=68.5$ cm^{-1}, $\omega_8=56$ cm^{-1}, and $\omega_7=46$ cm^{-1}) are strong and exhibit a quasiquadratic field dependence. There is a mode that extrapolates to $\omega_5=29$ cm^{-1} at zero field. This mode (mode 5) seems to be activated as mode 3 (starting at $\omega_3=24.4$ cm^{-1} becomes inactive). For field along **b** and polarization along **a** there is another weak mode that disappears at low fields; this mode extrapolates to $\omega_4=25.5$ cm^{-1}. The field dependence of this mode (mode 4) makes it clearly distinct from mode 3. Mode 2 is approximately independent of the field. The most prominent feature is mode 1, starting at $\omega_1=13.5$ cm^{-1} and curving upwards. Note that this mode actually crosses mode 2 around

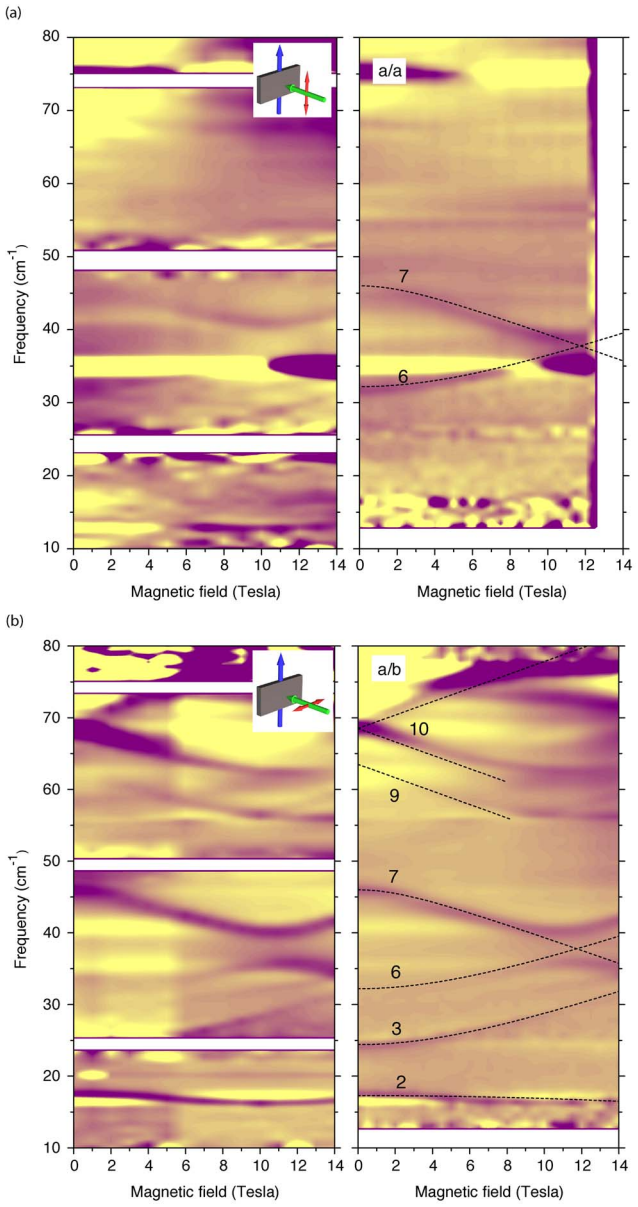

FIG. 4. (Color online) Intensity maps for external field along the **a** direction, for two polarizations of the incident light: parallel to **a** [(a)] and parallel to **b** [(b)]. For each setting the measurement was done with the mylar (left) and with the Ge-coated mylar (right) beamsplitters. There was a technical problem with the data collection for the second panel from the right, and the data for fields greater than 12 T are not valid. Lines are fits described in Appendix A.

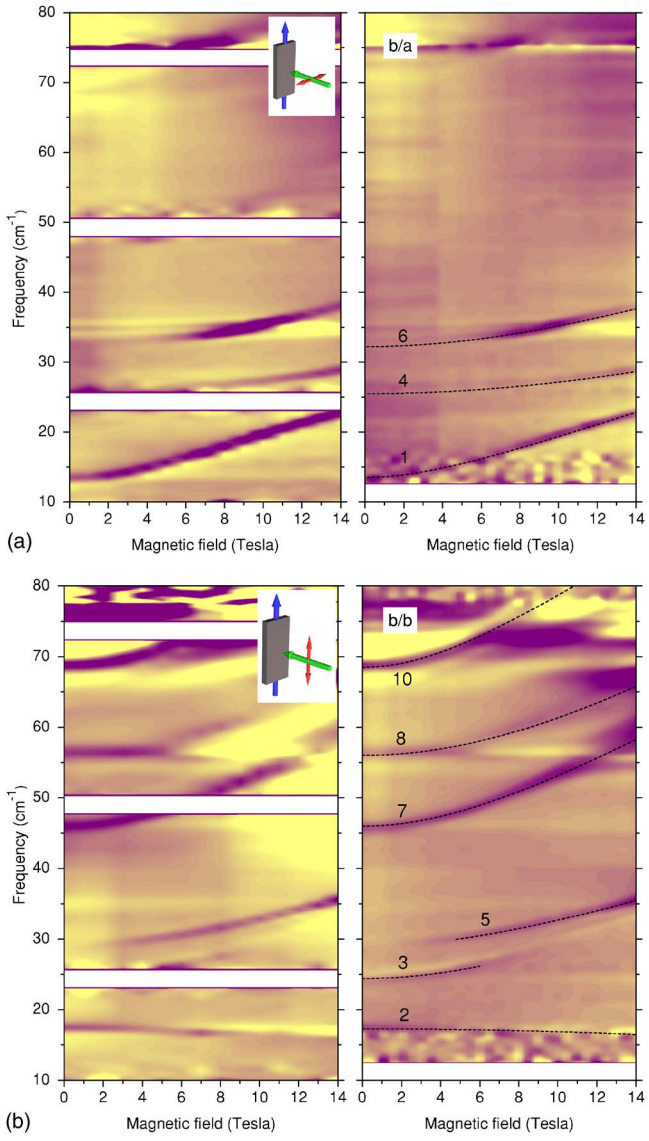

FIG. 5. (Color online) Intensity maps for external field along the **b** direction, for two polarizations of the incident light: parallel to **a** [(a)] and parallel to **b** [(b)]. For each setting the measurement was done with the mylar (left) and with the Ge-coated mylar (right) beamsplitters. Lines are fits described in Appendix A.

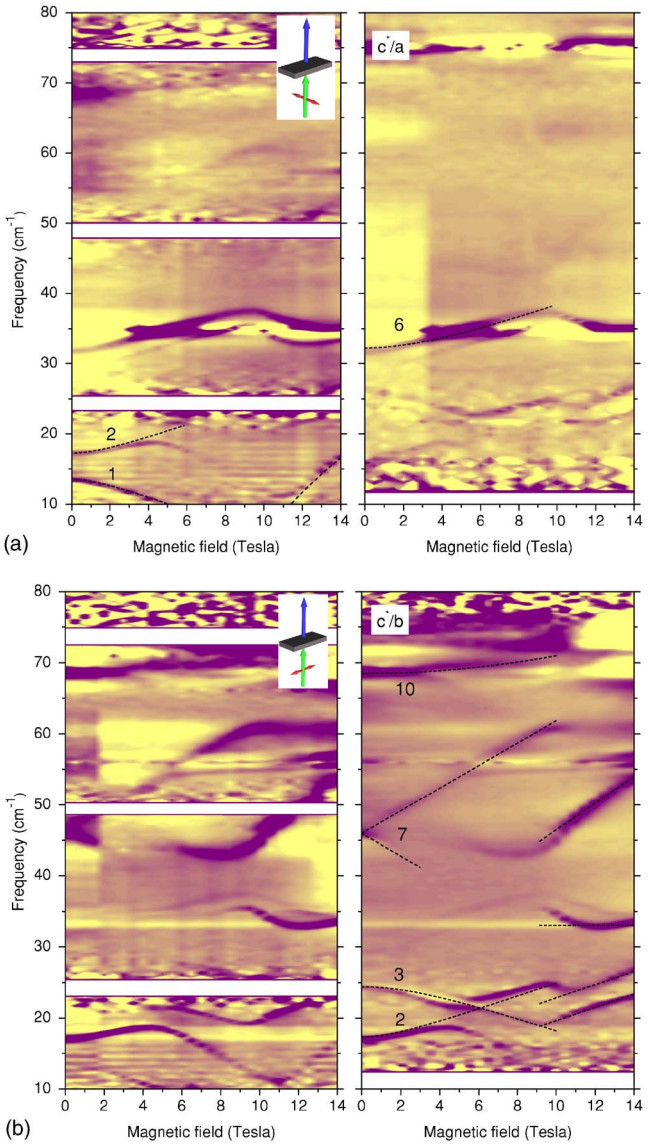

FIG. 6. (Color online) Intensity maps for external field perpendicular to the **a**-**b** plane, for two polarizations of the incident light: parallel to **a** [(a)] and parallel to **b** [(b)]. For each setting the measurement was done with the mylar (left) and with the Ge-coated mylar (right) beamsplitters. Lines are fits described in Appendix A.

5 T. There is absolutely no evidence of interaction between these two modes, and the two modes are excited with different polarizations. This leads to the conclusion that these modes are orthogonal even in finite fields.

When the field is applied perpendicular to the **a**-**b** plane, the spin order suffers a field-induced transition around 9 T (Fig. 6). For low fields modes 1, 2, and 6 are visible for polarization along the **a** direction; modes 2, 3, 7, and 10 are active for the other polarization direction. Modes 2 and 3 cross and interact strongly between 4 and 6 T. Mode 7 (starting at ω_7=46 cm^{-1}) splits upon the application of the field, but the intensity of the lower branch disappears rapidly.

Somewhere between 9 and 10 T all modes exhibit a dramatic change. Mode 1, that started to soften with increasing field, probably reaches zero frequency in this field range. The mode is recovered in the measured field and frequency domain at 11 T, approaching 16 cm^{-1} at 14 T. New modes appear around 20 and 34 cm^{-1}; other modes exhibit a sudden jump in frequency. The field-induced transition seen here is similar to the spin-flop transition well known in simple antiferromagnets and will be discussed later.

In a quasiclassical picture the spin-resonance modes are determined by the equations of motion; in the most general case this is equivalent to finding the eigenvalues of a $2m \times 2m$ matrix, where m is the number of sublattices. Half of the eigenvalues are positive, corresponding to the spin-resonance frequencies. The quantum-mechanical treatment leads to an identical problem in the linear approximation.[7] Accordingly, there are four modes in orthoferrites[8] and six modes in triangular magnets.[2] In $Ni_5(TeO_3)_4Cl_2$ there are 20 Ni ions in the unit cell, ten on each of the two NiO sheets

TABLE I. Zero-field modes derived form the field dependence measured in all field directions. Twofold degeneracy means that the resonance splits into two lines in at least one field direction. The "field/polarization" entry refers to the scan where the mode was seen: The direction of the static field and the direction of the oscillating magnetic field relative to the sample are indicated ($\mathbf{c}^*$ is perpendicular to directions **a** and **b**). "HF" means that the mode is only visible at high fields, and the zero-field frequency was determined by extrapolation.

Mode	1	2	3	4	5	6	7	8	9	10
Frequency	13.5 cm^{-1}	17.3 cm^{-1}	24.4 cm^{-1}	25.5 cm^{-1}	29 cm^{-1}	32.2 cm^{-1}	46 cm^{-1}	56 cm^{-1}	63 cm^{-1}	68.5 cm^{-1}
Degeneracy	1	1	1	1	1	1	2	1	1	2
Field/ polarization	b/a, c^*/a	a/b, b/b, c^*/a, c^*/b	a/b, b/b, c^*/b	b/a HF	b/b HF	a/a, a/b HF, b/a HF, c^*/a	a/a, a/b, b/b, c^*/b	b/b	a/b HF	a/b, b/b, c^*/b

(see Fig. 1). The coupling is expected to be weak between the sheets, and one can focus on the exchange parameters between the ten Ni atoms on a single sheet in the unit cell. One can envision an antiferromagnetic structure with ten magnetic sublattices, each one belonging to one Ni ion. The magnetic ground state is determined by the balance of exchange, anisotropy and Dzyaloshinski-Moriya (DM) interactions. A total of ten spin-resonance modes in this model would be consistent with the experimental results. At least eight of these modes can be clearly identified in the measurement. Modes 1,2 and 3,6 are split pairs in zero field. Modes 7 and 10 are degenerate in zero field, but two frequencies can be distinguished in finite fields for at least one field direction. (Notice that the lower branch of Mode 7 loses its intensity as the field is increased. Nevertheless, for low fields the splitting of the mode is beyond doubt, see Fig. 6.) The ninth mode has $\omega_8 = 56$ cm^{-1} at zero field.

Modes 4, 5 (see Fig. 5), and 9 (see Fig. 4) appear gradually at finite fields. Even if one assumes that a mode has exactly zero intensity in zero external field one may not conclude that the mode does not exist. The mode could be seen by other methods, e.g., by neutron spectroscopy. (Perhaps the best analogy is the $\mathbf{k}=0$ optical-phonon mode in a silicon or diamond: This mode is not seen in optical spectroscopy, since the dipole moment of the oscillation is exactly zero by symmetry.) Even if the ESR line transition is not forbidden in zero field, its intensity may be very weak. Strongly field-dependent intensity for an allowed spin-resonance mode has been observed before, for example in the quasi-one-dimensional helimagnet $LiCu_2O_2$.[9] Therefore we cannot say for sure if any of these modes are truly absent in zero field. However, in two out of the three cases a correlated diminishing of intensity seems to exist in another mode: Mode 5 gains intensity as mode 3 disappears. Mode 9 and the lower branch of mode 10 exhibits similar behavior. It is tempting to conclude that the magnetic field induces some type of crossover behavior, and modes 5 and 9 are not distinct modes existing at zero field as well. If that is true, than the tenth mode is mode 4.

Strong phonon absorption makes the ESR studies at higher frequencies impossible, except for a narrow frequency range between 110 and 120 cm^{-1}. (That range is not shown in the figures, but no magnetic absorption was observed here.) Do we expect to find more magnon modes at frequencies above the measured range? The answer is most likely no. For the lowest energy modes, the ESR frequency is strongly influenced by the anisotropy; in the absence of single-ion or exchange anisotropy these modes would be at zero frequency. For the other modes, however, the frequency is mostly determined by the exchange couplings. Although we know relatively little about the microscopic parameters of our material, the energy scale of the exchange couplings can be estimated from the phase-transition temperature of 25 K, and we get $H_E \sim 20$ cm^{-1}. Frustrated coupling and competing interactions can suppress the phase-transition temperature, but it is unlikely that any given exchange energy is larger than a few times of 20 cm^{-1}. This sets the upper cutoff frequency for the magnon modes nicely within our range of measurement. The properties of magnets with the garnet structure, where the magnetic order is similarly complex, support this argument. (For example, in $Mn_3Al_2Ge_3O_{12}$, recently studied by inelastic neutron scattering,[10] there are eight sublattices and magnon modes, with the highest frequency mode at 8 cm^{-1}. The phase-transition temperature of this compound is 6.8 K.) The same conclusion can be drawn from the model discussed below.

III. THEORY

Antiferromagnetic resonance in the presence of uniaxial easy axis anisotropy was described by Keffer and Kittel.[11] In the simplest case there are two relevant parameters: the exchange field H_E, characteristic of the interaction between the spins, and the anisotropy field H_A, setting the preferred spin direction relative to the lattice. The spin-resonance frequency in zero field is $\omega_0 = \gamma\sqrt{H_A(H_A+2H_E)} \approx \gamma\sqrt{2H_AH_E}$, since typically $H_A \ll H_E$. When the external field is parallel to the easy axis, this line splits in two, and the corresponding frequencies follow $\omega = \omega_0 \pm \gamma H$. In high field, at $H_{EA} = \omega_0/\gamma$, the orientation of the spins changes in a process called the spin-flop transition. At fields above H_{EA} there are two new resonance modes, one at zero frequency and the other one at $\omega = \gamma\sqrt{H^2 - H_{EA}^2}$. For fields perpendicular to the easy axis one of the modes is independent of the frequency and the other one behaves as $\omega = \gamma\sqrt{H^2 + H_{EA}^2}$. Nagamiya[12] treated the same model with general (bi-axial) anisotropy, as discussed later in greater detail. The main finding is that the zero-field mode is split, and for fields parallel to the easy axis the magnetic-field dependence of the two frequencies can be described, in a good approximation for low fields, as $\omega = \omega_0 \pm \sqrt{H^2 + H_1^2}$ (here H_1 characterizes the weaker anisotropy within the plane perpendicular to the easy axis). The two-sublattice model with Dzyaloshinski-Moriya (DM) interaction was

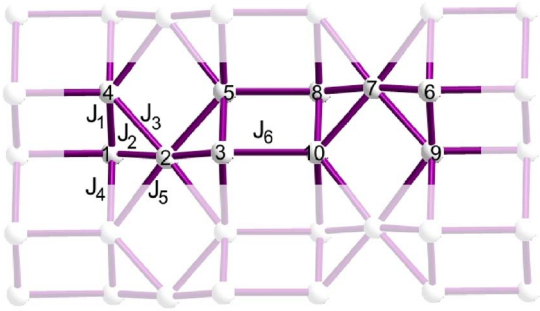

FIG. 7. (Color online) Ni ion network within a single layer, viewed from the [101] direction in the crystal. Darker shades represent ions in a single unit cell. In this view the "buckling" of the Ni ions (apparent in Fig. 1) is not visible, and the structure looks especially simple. The exchange couplings and the indices for the Ni ions used in the model Hamiltonian are also indicated.

treated by Seehra and Castner,[13] and more recently by Mukhin *et al.*[14] The DM coupling also removes the zero-field degeneracy and for fields parallel to the easy axis the mode frequencies follow a similar expression, $\omega=\omega_0\pm\sqrt{H^2+H_1^2}$, where H_1 characterizes the DM coupling, assumed to be small here. In Turov's review[15] saturation effects are also discussed. Saturation occurs when the external field is close to and exceeds the exchange field. The resonance modes that start out to be independent of frequency at low fields are the most sensitive to saturation effects, and the frequency dependence follows $\omega=\omega_0\sqrt{1-(H/H_E)^2}$. The slow decrease of the frequency of the ω_2 mode in for fields parallel to **a** and **b** may be due to saturation effects. Herrmann[8] discussed orthoferrites, with a more complicated magnetic structure of four sublattices. The Japanese school studied triangular antiferromagnets with six sublattices,[16] as reviewed by Tanaka and co-workers.[2]

In a general sense the two low-energy modes in Fig. 6 follow the behavior seen in a two-sublattice, biaxial antiferromagnet,[12] with the easy direction identified as $\mathbf{c}^*$. For fields parallel to $\mathbf{c}^*$ the frequency of mode 1 decreases, and the frequency of mode 2 increases. For fields perpendicular to $\mathbf{c}^*$ one of the mode frequencies is approximately independent of the field (Figs. 4 and 5).

The observation of ten spin-resonance modes suggests that a model Hamiltonian must deal with ten spin sublattices in this material. The bonds between the Ni atoms have no particular symmetries restricting the nature of the exchange interactions. At this stage, in the absence of information about the orientation of the spins, one cannot attempt to refine all of the possible exchange parameters. Instead, we set a limited goal: We will reduce the number of parameters as much as possible, and we will show that the low-energy spectrum, including the spin-flop transition, is described by a reasonable set of exchange couplings.

We will assume that the interaction between spins separated by the Cl layers in the structure is weak, and the system is quasi-two-dimensional. The unit cell of a single NiO layer is shown in Fig. 7. We introduce exchange couplings, labeled in the order of increasing bond lengths (see also Fig. 1), but we will neglect the second-neighbor couplings J_3 and J_5. We will also neglect the single-ion spin anisotropy that is usually much smaller than the exchange anisotropy. The Hamiltonian is given by

$$
\begin{aligned}
H=\sum_{\mathbf{r}}(&\mathbf{S}_{1,\mathbf{r}}\overleftrightarrow{J}_1\mathbf{S}_{4,\mathbf{r}}+\mathbf{S}_{3,\mathbf{r}}\overleftrightarrow{J}_1\mathbf{S}_{5,\mathbf{r}}+\mathbf{S}_{8,\mathbf{r}}\overleftrightarrow{J}_1\mathbf{S}_{10,\mathbf{r}}+\mathbf{S}_{6,\mathbf{r}}\overleftrightarrow{J}_1\mathbf{S}_{9,\mathbf{r}}\\
&+\mathbf{S}_{1,\mathbf{r}}\overleftrightarrow{J}_2\mathbf{S}_{2,\mathbf{r}}+\mathbf{S}_{2,\mathbf{r}}\overleftrightarrow{J}_2\mathbf{S}_{3,\mathbf{r}}+\mathbf{S}_{7,\mathbf{r}}\overleftrightarrow{J}_2\mathbf{S}_{8,\mathbf{r}}+\mathbf{S}_{6,\mathbf{r}}\overleftrightarrow{J}_2\mathbf{S}_{7,\mathbf{r}}\\
&+\mathbf{S}_{4,\mathbf{r}}\overleftrightarrow{J}_4\mathbf{S}_{1,\mathbf{r}-\mathbf{a}_y}+\mathbf{S}_{5,\mathbf{r}}\overleftrightarrow{J}_4\mathbf{S}_{3,\mathbf{r}-\mathbf{a}_y}+\mathbf{S}_{8,\mathbf{r}}\overleftrightarrow{J}_4\mathbf{S}_{10,\mathbf{r}-\mathbf{a}_y}\\
&+\mathbf{S}_{6,\mathbf{r}}\overleftrightarrow{J}_4\mathbf{S}_{9,\mathbf{r}-\mathbf{a}_y}+\mathbf{S}_{3,\mathbf{r}}\overleftrightarrow{J}_6\mathbf{S}_{10,\mathbf{r}}+\mathbf{S}_{5,\mathbf{r}}\overleftrightarrow{J}_6\mathbf{S}_{8,\mathbf{r}}+\mathbf{S}_{6,\mathbf{r}}\overleftrightarrow{J}_6\mathbf{S}_{4,\mathbf{r}+\mathbf{a}_x}\\
&+\mathbf{S}_{9,\mathbf{r}}\overleftrightarrow{J}_6\mathbf{S}_{1,\mathbf{r}+\mathbf{a}_x}),
\end{aligned}
\tag{1}
$$

where $\mathbf{r}$ denotes the position of the unit cell, $\mathbf{a}_{x,y}$ are the nearest-neighbor lattice vectors. The $\overleftrightarrow{J}$ matrices represent the exchange interactions; in the absence of symmetries this tensor will have components representing the DM interaction as well. This leaves us with a very large number of coupling parameters. To simplify the model, both the symmetric[17] and the antisymmetric DM interactions are neglected, and the principal axes of all tensors are assumed to be collinear and coincide with the crystallographic **a**, **b**, and $\mathbf{c}^*$ directions. In this approximation, each exchange coupling can be represented by three numbers, J^x, J^y, J^z, the diagonal components of tensor $\overleftrightarrow{J}$. For the calculation of the energy spectrum at zero wave number the exchange couplings J_1 and J_4 can be merged into one effective coupling, $J_1'=J_1+J_4$. This leaves us with nine independent coupling constants.

Complex spin ground states with noncollinear spin orientations are possible even in this simplified model. Searching the full parameter space is not practical. However, the number of possible ground states is dramatically reduced if we assume that all spins are collinear. In our case the direction of all spins is assumed to be either parallel or antiparallel to $\mathbf{c}^*$. This assumption is not entirely consistent with the experiment, since the splitting of the highest energy mode in fields along the **a** direction (Fig. 4) is characteristic of spin orientations collinear of **a**. Nevertheless, the approximation was necessary in order to make the calculation manageable, and it is acceptable when we are interested in the field dependence of the low-energy modes only.

Magnetization measurements indicate that in the ordered state there is no ferromagnetic moment.[4] Therefore the ground-state configurations for collinear spins are limited to four possibilities, illustrated in Fig. 8.

In the simplified Hamiltonian investigated here the diagonal couplings (dashed lines) are assumed to be zero. In this approximation configuration 1 can be transformed into configuration 2 by the interchange of the J_6 and the J_1+J_4 couplings. A similar equivalence transformation applies between configurations 3 and 4. This leaves us with two inherently different spin configurations. Each configuration places particular restrictions of the sign and anisotropy of the exchange parameters.

A broad search of the nine-parameter space for configurations 2 and 4 was performed. The magnon spectrum was determined by diagonalizing the Hamiltonian, obtained in the linear approximation after a Holstein-Primakoff transfor-

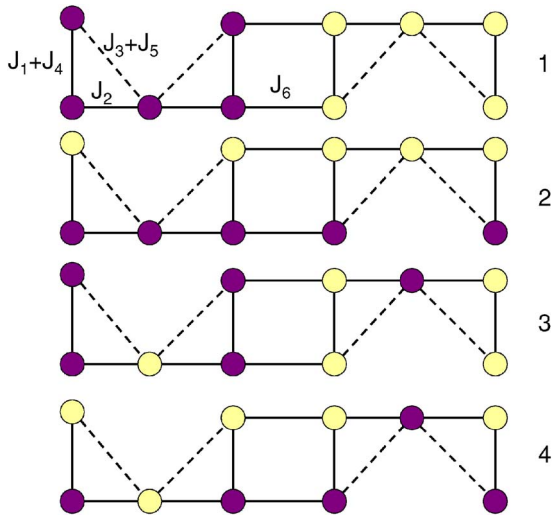

FIG. 8. (Color online) Unit cells for the four possible spin configurations, numbered 1–4 on the right side. Uniaxial exchange anisotropy is assumed, so that all spins are collinear. Dark and light colors correspond to the two possible spin orientations. The effective couplings strengths for the long-wavelength ($q=0$) magnon modes are also shown.

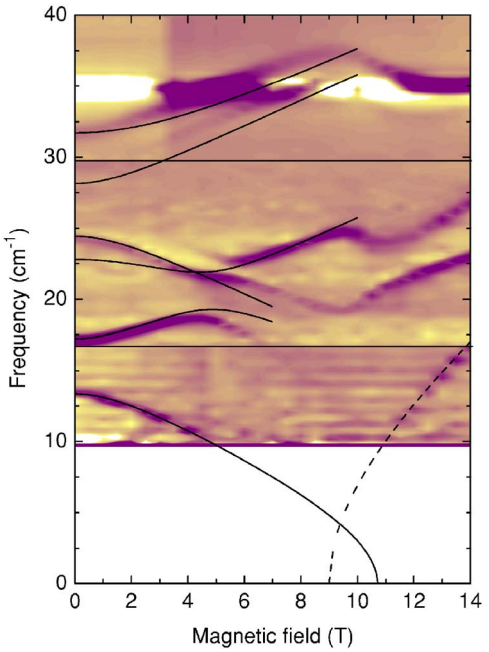

FIG. 9. (Color online) Experimental data merged from three data sets shown in Fig. 6, and the theoretical results (continuous lines). The dashed line represents the empirical fit to the lowest energy mode for fields higher than the spin-flop field, as described in Appendix A.

mation. The details of the calculation are described in Appendix B. In selecting the possible exchange couplings we attempted to make them the "most isotropic" i.e., we tried to make the components of a $\overleftrightarrow{J}$ tensor equal to each other. We quickly found that some features of the two-sublattice models appear in our model as well. For example, if only uniaxial anisotropy was allowed, than the lowest two modes were degenerate in zero field, $\omega_1=\omega_2$. (With no anisotropy the lowest mode frequency was zero, as expected for a rotationally invariant Hamiltonian.) Therefore it became clear that the minimum number of parameters required to fit the experiments is 5 (three exchange couplings and two anisotropies). It turns out that the minimum number of parameters yields a surprisingly good agreement as well, at least for the low-lying modes.

The best agreement (shown in Fig. 9, with parameters listed in Table II) was obtained for configuration 2. The calculation reproduces the zero-field frequencies, the crossover of the three modes around 5 T, and the expected dramatic drop of the lowest magnon frequency (a precursor to the spin-flop transition) around 10 T. This latter feature is particularly nontrivial. In simple antiferromagnets there is a rather strict scaling between the frequency of the zero-field mode and the spin-flop field, yielding a much larger spin-flop field (around 14.5 T) than the observed one.

The eigenvector belonging to the lowest-lying mode has interesting symmetries. The spin-pairs 1,3; 4,5; 6,8; and 9,10 have identical motion in any field. In zero field, spin pairs 3,8; 1,6; 4,9; and 5,10 have exactly opposite motion. Close to the spin-flop field the amplitude of the motion for spins 6, 7, 8 approaches zero.

According to this result, the spins responsible for the spin-flop transition and the six low-lying modes are collinear to the $\mathbf{c}^*$ direction (the $\mathbf{z}$ direction of the reference frame used for the exchange tensors). The strongest coupling is isotropic; the other two couplings have an "easy plane" character, but the two planes are perpendicular to each other. The combined effect of these anisotropies is an effective "easy axis" for the coupled spin system. Notice that the spin-flop transition at relatively low fields, as observed experimentally, is related to this feature of the exchange parameters. When we attempted to fit the data with biaxial anisotropy for one of the exchange couplings, we obtained much higher spin-flop fields (with similar good agreement for the zero-field frequencies).

In summary, the electron spin resonance on this complex material has ten modes, and each line exhibits a characteristic magnetic-field dependence. Mode counting arguments lead to the conclusion that the magnetic unit cell in the ordered phase is the same as the structural unit cell. The field induced transition in the magnetic-resonance features is analogous to the spin-flop transition well known for the two-sublattice, easy axis antiferromagnets. The relatively small spin-flop field in this compound is most likely related to the fact that the dominant anisotropy in this spin system is the result of two intersecting easy-plane anisotropies acting in

TABLE II. Diagonal components of the exchange tensors (in units of cm^{-1}) belonging the curves in Fig. 9. Negative values indicate ferromagnetic couplings.

	J_1'	J_2	J_6
x	33.2	−26.4	−2.06
y	33.2	−15.9	−6.25
z	33.2	−26.4	−6.25

TABLE III. Empirical fits to the low-field spin-resonance modes. The numbers represent frequencies in cm^{-1}. H denotes the magnetic field, converted to frequency by $H[cm^{-1}]=0.934\ cm^{-1}\ T^{-1}H[T]$.

Mode	$\mathbf{H}_0\|\mathbf{a}$	$\mathbf{H}_0\|\mathbf{b}$	$H_0\perp\mathbf{a}-\mathbf{b}$
ω_1		$9.0+\sqrt{4.5^2+H^2}$	$15.4-\sqrt{1.9^2+H^2}$
ω_2	$\sqrt{17.3^2-(0.4H)^2}$	$\sqrt{17.3^2-(0.4H)^2}$	$15.4+\sqrt{1.9^2+H^2}$
ω_3	$16.4+\sqrt{8^2+H^2}$ or $\sqrt{24.4^2+(1.6H)^2}$	$16.4+\sqrt{8^2+H^2}$ or $\sqrt{24.4^2+(1.6H)^2}$	$28.3-\sqrt{3.9^2+H^2}$
ω_4		HF: $\sqrt{25.5^2+H^2}$	
ω_5		HF: $19+\sqrt{10^2+H^2}$ or $\sqrt{29^2+(1.6H)^2}$	
ω_6	HF: $24.2+\sqrt{8^2+H^2}$ or $\sqrt{32.2^2+(1.9H)^2}$	HF: $19.2+\sqrt{13^2+H^2}-13$ or $\sqrt{32.2^2+(1.5H)^2}$	$28.3+\sqrt{3.9^2+H^2}$
ω_7	$42.5-\sqrt{3.5^2+H^2}$	$32+\sqrt{14^2+(1.7H)^2}$ or $\sqrt{46^2+(2.8H)^2}$	$46\pm1.7H$
ω_8		$26+\sqrt{30^2+(2H)^2}$ or $\sqrt{56^2+(2.7H)^2}$	
ω_9	HF: $63-H$		
ω_{10}	$68.5\pm H$	$56.5+\sqrt{12^2+(2H)^2}$ or $\sqrt{68.5^2+(4.1H)^2}$	$\sqrt{68.5^2+(2H)^2}$

two different exchange couplings. While the two-dimensional model discussed here correctly reproduces some of the nontrivial properties of the low-energy excitations, the model is not complete: it is possible that the spins are not collinear, the parameters J_3 and J_5 may be finite, and interlayer coupling is important for the relatively high magnetic transition temperature. Further investigations, including the determination of the magnetic structure by neutron scattering, is necessary for the complete exploration of this compound.

ACKNOWLEDGMENTS

We are indebted to D. Ariosa (EPFL) for the x-ray characterization of the sample, and G. L. Carr (BNL) for valuable discussions and for developing the IR facilities at the NSLS. This work was supported by the Hungarian Research Fund OTKA TS 049881, NDF 45172, PF 63954, and NK 60984, by the Swiss NSF, and its NCCR "MaNEP." L.M. received support in the Szent-Györgyi program from the Hungarian Ministry of Education. B.D. acknowledges the Magyary program (MZFK) for support. Use of the National Synchrotron Light Source, Brookhaven National Laboratory, was supported by the U.S. Department of Energy, Office of Science, Office of Basic Energy Sciences, under Contract No. DE-AC02-98CH10886.

APPENDIX A

Motivated by the characteristic behavior of the two-sublattice systems, as discussed above, we performed two-parameter fits to the observed field dependencies of the resonance lines. (For noninteracting spins the spin-resonance frequency is $\omega=\gamma H$ where $\gamma=g\mu_B/\hbar$ with g being the so-called g factor, and μ_B is the Bohr magneton. For the free spin g factor of 2 one gets $\gamma=0.934\ cm^{-1}\ T^{-1}$. We will use this coefficient to convert all fields to frequencies, and drop the factor γ from the equations.) For modes that are nearly independent of field we used $\omega=H_0\sqrt{1-(H/H_E)^2}$ representing saturation behavior.[15] For modes that seem to appear as pairs we used either $\omega=\omega_0\pm\alpha H$ or, if the pair was split in zero field, $\omega=\omega_0\pm\sqrt{H^2+H_1^2}$. We attempted to fit all other modes with two expressions, called type A and type B, respectively:

$$\omega=\sqrt{(\alpha H)^2+H_1^2}\quad\text{or}\quad\omega=\omega_0\pm\sqrt{(\alpha H)^2+H_1^2}. \tag{A1}$$

Note that in our units $\alpha=1$ (no pre-factor in H) means the regular g factor of 2.

The empirical fits to the field dependence of the modes are listed in Table III, and indicated in the figures by dashed lines. Type-A and -B fits were well within the experimental linewidth in most cases, except for the ω_1 mode with $H_0\|b$, when the type-A fit does not work. In type-B fits we fixed $\alpha=1$, if possible, and H_1 and ω_0 were the fitting parameters. For the high-frequency modes the type-B fits were possible only if $\alpha>1$ was allowed; in this case the three-parameter fit is not unique, and other combinations of ω_0, α and H_1 may work equally well.

Turov[15] discussed saturation effects, i.e., the behavior of the spin-resonance lines when the applied magnetic field is comparable to the exchange field, and all spins line up parallel to the external field. The typical field dependence of the frequency obtained in this case is $\omega=\omega_0\sqrt{1-(H/H_E)^2}$. Comparing this expression to the behavior of the ω_2 mode for fields parallel to **a** or **b**, one obtains a saturation field of $H_E=43.25\ cm^{-1}=46.3$ T. This value is comparable to the exchange couplings obtained independently for the spin Hamiltonian Eq. (1).

In the high-field regime of Fig. 6 the dotted lines represent empirical fits for the modes, corresponding to equations $\omega=37+2H$; $\omega=13.5+H$; $\omega=33$ $\omega=10.3+H$; $\omega=1.7\sqrt{H^2-(0.934\times9)^2}$.

APPENDIX B

Holstein-Primakoff transformation has been performed on the Hamiltonian Eq. (1). With the introduction of matrices

$$D_2=\begin{bmatrix}-2J_2^z & 0\\ 0 & -2J_2^z\end{bmatrix}, \tag{B1}$$

$$D_3=\begin{bmatrix}J_1'^z-J_6^z & 0\\ 0 & J_1'^z-J_6^z\end{bmatrix}, \tag{B2}$$

$$D_4 = \begin{bmatrix} J_1'^z - J_2^z - J_6^z & 0 \\ 0 & J_1'^z - J_2^z - J_6^z \end{bmatrix}, \tag{B3}$$

$$O_6 = \begin{bmatrix} (J_6'^x + J_6'^y)/2 & (J_6'^x - J_6'^y)/2 \\ (J_6'^x - J_6'^y)/2 & (J_6'^x + J_6'^y)/2 \end{bmatrix}, \tag{B4}$$

$$O_2 = \begin{bmatrix} (J_2^x + J_2^y)/2 & (J_2^x - J_2^y)/2 \\ (J_2^x - J_2^y)/2 & (J_2^x + J_2^y)/2 \end{bmatrix}, \tag{B5}$$

$$O_1 = \begin{bmatrix} (J_1^x - J_1^y)/2 & (J_1^x + J_1^y)/2 \\ (J_1^x + J_1^y)/2 & (J_1^x - J_1^y)/2 \end{bmatrix}, \tag{B6}$$

the Hamiltonian can be brought to matrix form as

$$H = \begin{bmatrix} D_4 - gh & O_2 & 0 & O_1 & 0 & 0 & 0 & 0 & O_6 & 0 \\ O_2 & D_2 - gh & O_2 & 0 & 0 & 0 & 0 & 0 & 0 & 0 \\ 0 & O_2 & D_4 - gh & 0 & O_1 & 0 & 0 & 0 & 0 & O_6 \\ O_1 & 0 & 0 & D_3 + gh & 0 & O_6 & 0 & 0 & 0 & 0 \\ 0 & 0 & O_1 & 0 & D_3 + gh & 0 & 0 & O_6 & 0 & 0 \\ 0 & 0 & 0 & O_6 & 0 & D_4 + gh & O_2 & 0 & O_1 & 0 \\ 0 & 0 & 0 & 0 & 0 & O_2 & D_2 + gh & O_2 & 0 & 0 \\ 0 & 0 & 0 & 0 & O_6 & 0 & O_2 & D_4 + gh & 0 & O_1 \\ O_6 & 0 & 0 & 0 & 0 & O_1 & 0 & 0 & D_3 - gh & 0 \\ 0 & 0 & O_6 & 0 & 0 & 0 & 0 & O_1 & 0 & D_3 - gh \end{bmatrix}, \tag{B7}$$

where gh denotes the applied magnetic field. This matrix acts on the space of Holstein boson creation and annihilation operators. To obtain the energy spectrum, one has to introduce the metric matrix G, composed of ± 1 along the diagonal in an alternating fashion.[7] The matrix to be diagonalized is GH, whose positive eigenvalues give the energy gaps.

[1] For a historical introduction, see Claire L'huillier, cond-mat/0502464 (unpublished).

[2] H. Tanaka, T. Ono, S. Maruyama, S. Teraoka, K. Nagata, H. Ohta, S. Okubo, S. Kimura, T. Kambe, H. Nojiri, and M. Motokawa, J. Phys. Soc. Jpn. **72** Suppl. B, 84 (2003).

[3] D. Talbayev, L. Mihály, and J. Zhou, Phys. Rev. Lett. **93**, 017202 (2004); L. Mihály, D. Talbayev, L. F. Kiss, J. Zhou, T. Fehér, and A. Jánossy, Phys. Rev. B **69**, 024414 (2004).

[4] M. Johnsson, K. W. Tornroos, P. Lemmens, and P. Millet, Chem. Mater. **15**, 68 (2003).

[5] G. L. Carr (private communication).

[6] A. F. Garcia-Flores, E. Granado, H. Martinho, R. R. Urbano, C. Rettori, E. I. Golovenchits, V. A. Sanina, S. B. Oseroff, S. Park, and S.-W. Cheong, Phys. Rev. B **73**, 104411 (2006).

[7] M. E. Zhitomirsky and I. A. Zaliznyak, Phys. Rev. B **53**, 3428 (1996).

[8] G. Herrmann, Phys. Rev. **133**, A1334 (1964).

[9] L. Mihály, B. Dóra, A. Ványolos, H. Berger, and L. Forró, Phys. Rev. Lett. **97**, 067206 (2006).

[10] A. Gukasov, V. P. Plakhty, B. Dorner, S. Yu. Kokovin, V. N. Syromyatnikov, O. P. Smirnov, and Yu. P. Chernenkov, J. Phys.: Condens. Matter **11**, 2869 (1999).

[11] F. Keffer and C. Kittel, Phys. Rev. **85**, 329 (1952).

[12] T. Nagamiya, Prog. Theor. Phys. **11**, 309 (1954).

[13] M. Seehra and T. G. Castner, Phys. Rev. B **1**, 2289 (1970).

[14] A. A. Mukhin, V. Yu. Ivanov, V. D. Travkin, A. Pimenov, A. Loidl, and A. M. Balbashov, Europhys. Lett. **49**, 514 (2000).

[15] E. A. Turov, *Physical Properties of Magnetically Ordered Crystals* (Academic, New York, 1965).

[16] T. Kambe, H. Tanaka, S. Kimura, H. Ohta, M. Motokawa, and K. Nagata, J. Phys. Soc. Jpn. **65**, 1799 (1996).

[17] L. Shekhtman, O. Entin-Wohlman, and A. Aharony, Phys. Rev. Lett. **69**, 836 (1992).